Hot-spot relaxation time current dependence in niobium nitride waveguide-integrated superconducting nanowire single-photon detectors

SIMONE FERRARI,[1,2,8] VADIM KOVALYUK,[3] WLADISLAW HARTMANN,[1,2] ANDREAS VETTER,[4,5] OLIVER KAHL,[1,2] CHANGHYOUP LEE,[5] ALEXANDER KORNEEV,[3,6] CARSTEN ROCKSTUHL,[4,5] GREGORY GOL'TSMAN,[3,6,7] AND WOLFRAM PERNICE[1,2,*]

[1]*University of Münster, Institute of Physics, Wilhelm-Klemm-Str. 10, 48149 Münster, Germany*
[2]*University of Münster, CeNTech - Center for Nanotechnology, Heisenbergstr. 11, 48149 Münster, Germany*
[3]*Moscow State Pedagogical University, Department of Physics, Moscow 119992, Russia*
[4]*Institute of Nanotechnology (INT), Karlsruhe Institute of Technology, 76344 Eggenstein-Leopoldshafen, Germany*
[5]*Institute of Theoretical Solid State Physics (TFP), Karlsruhe Institute of Technology, 76131 Karlsruhe, Germany*
[6]*Moscow Institute of Physics and Technology (State University), Moscow 141700, Russia*
[7]*National Research University Higher School of Economics, 20 Myasnitskaya Ulitsa, Moscow 101000, Russia*
[8]*simone.ferrari@uni-muenster.de*
[*]*wolfram.pernice@uni-muenster.de*

Abstract: We investigate how the bias current affects the hot-spot relaxation dynamics in niobium nitride. We use for this purpose a near-infrared pump-probe technique on a waveguide-integrated superconducting nanowire single-photon detector driven in the two-photon regime. We observe a strong increase in the picosecond relaxation time for higher bias currents. A minimum relaxation time of (22 ± 1) ps is obtained when applying a bias current of 50% of the switching current at 1.7 K bath temperature. We also propose a practical approach to accurately estimate the photon detection regimes based on the reconstruction of the measured detector tomography at different bias currents and for different illumination conditions.

References and links

1. G. N. Gol'tsman, O. Okunev, G. Chulkova, A. Lipatov, A. Semenov, K. Smirnov, B. Voronov, A. Dzardanov, C. Williams, and R. Sobolewski, "Picosecond superconducting single-photon optical detector," Appl. Phys. Lett. **79**(6), 705–707 (2001).
2. R. H. Hadfield, "Single-photon detectors for optical quantum information applications," Nat. Photonics **3**(12), 696–705 (2009).
3. F. Marsili, V. B. Verma, J. A. Stern, S. Harrington, A. E. Lita, T. Gerrits, I. Vayshenker, B. Baek, M. D. Shaw, R. P. Mirin, and S. W. Nam, "Detecting single infrared photons with 93% system efficiency," Nat. Photonics **7**(3), 210–214 (2013).
4. X. Hu, C. W. Holzwarth, D. Masciarelli, E. A. Dauler, and K. K. Berggren, "Efficiently coupling light to superconducting nanowire single-photon detectors," IEEE Trans. Appl. Supercond. **19**(3), 336–340 (2009).
5. J. P. Sprengers, A. Gaggero, D. Sahin, S. Jahanmirinejad, G. Frucci, F. Mattioli, R. Leoni, J. Beetz, M. Lermer, M. Kamp, S. Höfling, R. Sanjines, and A. Fiore, "Waveguide superconducting single-photon detectors for integrated quantum photonic circuits," Appl. Phys. Lett. **99**(18), 181110 (2011).

6. W. H. P. Pernice, C. Schuck, O. Minaeva, M. Li, G. N. Gol'tsman, A. V. Sergienko, and H. X. Tang, "High-speed and high-efficiency travelling wave single-photon detectors embedded in nanophotonic circuits," Nat. Commun. **3**, 1325 (2012).

7. O. Kahl, S. Ferrari, V. Kovalyuk, G. N. Gol'tsman, A. Korneev, and W. H. P. Pernice, "Waveguide integrated superconducting single-photon detectors with high internal quantum efficiency at telecom wavelengths," Sci. Rep. **5**, 10941 (2015).

8. J. L. O'Brien, "Optical Quantum Computing," Science **318**(5856), 1567–1570 (2007).

9. C. P. Dietrich, A. Fiore, M. G. Thompson, M. Kamp, and S. Höfling, "GaAs integrated quantum photonics: Towards compact and multi-functional quantum photonic integrated circuits," Laser Photonics Rev. **10**(6), 870–894 (2016).

10. S. Khasminskaya, F. Pyatkov, K. Słowik, S. Ferrari, O. Kahl, V. Kovalyuk, P. Rath, A. Vetter, F. Hennrich, M. M. Kappes, G. Gol'tsman, A. Korneev, C. Rockstuhl, R. Krupke, and W. H. P. Pernice, "Fully integrated quantum photonic circuit with an electrically driven light source," Nat. Photonics **10**(11), 727–732 (2016).

11. M. K. Akhlaghi, A. H. Majedi, and J. S. Lundeen, "Nonlinearity in single photon detection: modeling and quantum tomography," Opt. Express **19**(22), 21305–21312 (2011).

12. A. Engel, J. J. Renema, K. Il'in, and A. Semenov, "Detection mechanism of superconducting nanowire single-photon detectors," Supercond. Sci. Technol. **28**(11), 114003 (2015).

13. A. Divochiy, F. Marsili, D. Bitauld, A. Gaggero, R. Leoni, F. Mattioli, A. Korneev, V. Seleznev, N. Kaurova, O. Minaeva, G. Gol'tsman, K. G. Lagoudakis, M. Benkhaoul, F. Lévy, and A. Fiore, "Superconducting nanowire photon-number-resolving detector at telecommunication wavelengths," Nat. Photonics **2**(5), 302–306 (2008).

14. F. Marsili, D. Bitauld, A. Fiore, A. Gaggero, R. Leoni, F. Mattioli, A. Divochiy, A. Korneev, V. Seleznev, N. Kaurova, O. Minaeva, and G. Gol'tsman, "Superconducting parallel nanowire detector with photon number resolving functionality," J. Mod. Opt. **56**(2-3), 334–344 (2009).

15. D. Sahin, A. Gaggero, Z. Zhou, S. Jahanmirinejad, F. Mattioli, R. Leoni, J. Beetz, M. Lermer, M. Kamp, S. Höfling, and A. Fiore, "Waveguide photon-number-resolving detectors for quantum photonic integrated circuits," Appl. Phys. Lett. **103**(11), 111116 (2013).

16. D. Sahin, A. Gaggero, T. B. Hoang, G. Frucci, F. Mattioli, R. Leoni, J. Beetz, M. Lermer, M. Kamp, S. Höfling, and A. Fiore, "Integrated autocorrelator based on superconducting nanowires," Opt. Express **21**(9), 11162–11170 (2013).

17. M. S. Elezov, A. V. Semenov, P. P. An, M. A. Tarkhov, G. N. Gol'tsman, A. I. Kardakova, and A. Y. Kazakov, "Investigating the detection regimes of a superconducting single-photon detector," J. Opt. Technol. **80**(7), 435 (2013).

18. J. J. Renema, G. Frucci, Z. Zhou, F. Mattioli, A. Gaggero, R. Leoni, M. J. A. de Dood, A. Fiore, and M. P. van Exter, "Modified detector tomography technique applied to a superconducting multiphoton nanodetector," Opt. Express **20**(3), 2806–2813 (2012).

19. S. Ferrari, O. Kahl, V. Kovalyuk, G. N. Gol'tsman, A. Korneev, and W. H. P. Pernice, "Waveguide-integrated single- and multi-photon detection at telecom wavelengths using superconducting nanowires," Appl. Phys. Lett. **106**(15), 151101 (2015).

20. L. N. Bulaevskii, M. J. Graf, C. D. Batista, and V. G. Kogan, "Vortex-induced dissipation in narrow current-biased thin-film superconducting strips," Phys. Rev. B **83**(14), 144526 (2011).

21. A. N. Zotova and D. Y. Vodolazov, "Photon detection by current-carrying superconducting film: A time-dependent Ginzburg-Landau approach," Phys. Rev. B **85**(2), 024509 (2012).

22. R. Lusche, A. Semenov, K. Ilin, M. Siegel, Y. Korneeva, A. Trifonov, A. Korneev, G. Gol'tsman, D. Vodolazov, and H.-W. Hübers, "Effect of the wire width on the intrinsic detection efficiency of superconducting-nanowire single-photon detectors," J. Appl. Phys. **116**(4), 043906 (2014).

23. J. J. Renema, R. Gaudio, Q. Wang, Z. Zhou, A. Gaggero, F. Mattioli, R. Leoni, D. Sahin, M. J. A. de Dood, A. Fiore, and M. P. van Exter, "Experimental test of theories of the detection mechanism in a nanowire superconducting single photon detector," Phys. Rev. Lett. **112**(11), 117604 (2014).

24. F. Marsili, M. J. Stevens, A. Kozorezov, V. B. Verma, C. Lambert, J. A. Stern, R. D. Horansky, S. Dyer, S. Duff, D. P. Pappas, A. E. Lita, M. D. Shaw, R. P. Mirin, and S. W. Nam, "Hotspot relaxation dynamics in a current-carrying superconductor," Phys. Rev. B **93**(9), 094518 (2016).

25. J. J. Renema, R. Gaudio, Q. Wang, M. P. van Exter, A. Fiore, and M. J. A. de Dood, "Probing the hotspot interaction length in NbN nanowire superconducting single-photon detectors," https://arxiv.org/abs/1607.03088.

26. R. W. Heeres and V. Zwiller, "Superconducting detector dynamics studied by quantum pump-probe spectroscopy," Appl. Phys. Lett. **101**(11), 112603 (2012).

27. Z. Zhou, G. Frucci, F. Mattioli, A. Gaggero, R. Leoni, S. Jahanmirinejad, T. B. Hoang, and A. Fiore, "Ultrasensitive N-photon interferometric autocorrelator," Phys. Rev. Lett. **110**(13), 133605 (2013).

28. G. Di Giuseppe, M. Atatüre, M. D. Shaw, A. V. Sergienko, B. E. A. Saleh, M. C. Teich, A. J. Miller, S. W. Nam, and J. Martinis, "Direct observation of photon pairs at a single output port of a beam-splitter interferometer," Phys. Rev. A **68**(6), 063817 (2003).

29. A. G. Kozorezov, C. Lambert, F. Marsili, M. J. Stevens, V. B. Verma, J. A. Stern, R. Horansky, S. Dyer, S. Duff, D. P. Pappas, A. Lita, M. D. Shaw, R. P. Mirin, and S. W. Nam, "Quasiparticle recombination in hotspots in superconducting current-carrying nanowires," Phys. Rev. B **92**(6), 064504 (2015).

30. J. S. Lundeen, A. Feito, H. Coldenstrodt-Ronge, K. L. Pregnell, C. Silberhorn, T. C. Ralph, J. Eisert, M. B. Plenio, and I. A. Walmsley, "Tomography of quantum detectors," Nat. Phys. **5**(1), 27–30 (2009).
31. A. Feito, J. S. Lundeen, H. Coldenstrodt-Ronge, J. Eisert, M. B. Plenio, and I. A. Walmsley, "Measuring measurement: theory and practice," New J. Phys. **11**(9), 093038 (2009).
32. A. Korneev, Y. Korneeva, I. Florya, B. Voronov, and G. Gol'tsman, "NbN nanowire superconducting single-photon detector for mid-infrared," Phys. Procedia **36**, 72–76 (2012).
33. D. Bitauld, F. Marsili, A. Gaggero, F. Mattioli, R. Leoni, S. J. Nejad, F. Lévy, and A. Fiore, "Nanoscale optical detector with single-photon and multiphoton sensitivity," Nano Lett. **10**(8), 2977–2981 (2010).
34. A. Vetter, S. Ferrari, P. Rath, R. Alaee, O. Kahl, V. Kovalyuk, S. Diewald, G. N. Gol'tsman, A. Korneev, C. Rockstuhl, and W. H. P. Pernice, "Cavity-enhanced and ultrafast superconducting single-photon detectors," Nano Lett. **16**(11), 7085–7092 (2016).
35. A. D. Semenov, G. N. Gol'tsman, and A. A. Korneev, "Quantum detection by current carrying superconducting film," Phys. C Supercond. **351**(4), 349–356 (2001).
36. S. B. Kaplan, C. C. Chi, D. N. Langenberg, J. J. Chang, S. Jafarey, and D. J. Scalapino, "Quasiparticle and phonon lifetimes in superconductors," Phys. Rev. B **14**(11), 4854–4873 (1976).
37. R. Barends, J. J. A. Baselmans, S. J. C. Yates, J. R. Gao, J. N. Hovenier, and T. M. Klapwijk, "Quasiparticle relaxation in optically excited high-Q superconducting resonators," Phys. Rev. Lett. **100**(25), 257002 (2008).
38. M. Sidorova, A. Semenov, A. Korneev, G. Chulkova, Y. Korneeva, M. Mikhailov, A. Devizenko, A. Kozorezov, and G. Gol'tsman, "Electron-phonon relaxation time in ultrathin tungsten silicon film," https://arxiv.org/abs/1607.07321
39. Y. P. Gousev, G. N. Gol'tsman, A. D. Semenov, E. M. Gershenzon, R. S. Nebosis, M. A. Heusinger, and K. F. Renk, "Broadband ultrafast superconducting NbN detector for electromagnetic radiation," J. Appl. Phys. **75**(7), 3695–3697 (1994).
40. K. S. Il'in, M. Lindgren, M. Currie, A. D. Semenov, G. N. Gol'tsman, R. Sobolewski, S. I. Cherednichenko, and E. M. Gershenzon, "Picosecond hot-electron energy relaxation in NbN superconducting photodetectors," Appl. Phys. Lett. **76**(19), 2752–2754 (2000).

1. Introduction

Thanks to their high detection efficiency and outstanding timing characteristics, superconducting nanowire single-photon detectors (SNSPDs) have been established as a reliable solution for broadband optical detection of single photons, overcoming the limitation of more traditional solid state devices such as single-photon avalanche diodes, especially at telecom wavelengths [1–3]. SNSPDs integrated atop nanophotonic waveguides [4–7] represent a ready-to-use building block for quantum optical experiments on chip [8,9], enabling, for instance, correlation measurements and single-photon source characterization within integrated optics devices [10].

SNSPDs transduce the absorption of a photon in a recordable electric signal generated by the suppression of superconductivity in a localized region of a superconducting nanowire. Therefore SNSPDs act as binary (on-off) detectors [11]. This means that they are able to provide only two possible measurement outcomes: a recordable electric pulse or its absence. A detection event can be triggered by a real count, following the photon absorption in the nanowire, or to dark counts [12]. A non-recordable event, instead, can refer to the actual absence of a photon or to a situation in which an absorbed photon does not trigger a measurement signal because of insufficient deposited energy.

For many applications, photon-number resolving capabilities are desirable. Yet unless additional elements are introduced [13–16], SNSPDs cannot be directly used as photon-number resolving detectors. SNSPDs can be classified as threshold detectors. This suggests that, when operated at suitable conditions [1,17–19], they are able to distinguish only between the absorption of n photons or more, and less than n photons. This can be explained by considering the following detection mechanism model [12,19–23]: the absorption of a photon in a superconducting nanowire generates a localized cloud of excited quasiparticles, called a hot-spot, with higher temperature than the ground state Cooper pairs. The hot-spot enhances the entry of a single magnetic vortex or the generation of a vortex-antivortex pair (VAP). Driven by the Lorentz force, the single vortex or the VAP crosses the nanowire, generating a normal-state region. The breakdown of the superconductivity leads to the appearance of a finite resistance of the nanowire, thus resulting in a recordable voltage pulse. If the supercurrent density is not sufficiently large, after the formation of the hot-spot the

redistributed supercurrent density will not exceed the depairing current density, in which case the absorption of a single photon might not be sufficient for generating an output signal. Instead, the simultaneous absorption of two or more photons is required to achieve breakdown of the superconductivity. This is particularly true for low energy photons, such as telecom wavelength light around 1550 nm. In order that the multi-photon absorption generates a detection event, the consecutive absorption of individual photons has to occur not only in a limited region of the wire [24,25], but also in a timespan smaller than the original hot-spot lifetime (relaxation time) [19,24]. This peculiarity of SNSPDs represents a limit for the single-photon operation but, on the other hand, it allows us to exploit this characteristic as a multi-photon correlator [26,27], in analogy with successful application of Transition Edge Sensors (TES) [28]. Having a two-photon correlator consisting of one single detector is beneficial to overcome the time uncertainty limitation introduced by the jitter of two detectors and the correlation counter, typically present in standard correlation setups.

In order to design a two-photon autocorrelator, it is fundamental to have a detailed understanding of the dynamics of the hot-spot under different working conditions. Recent studies on WSi [24,29] demonstrate that bias current, wavelength, and temperature represent the three main parameters which affect the hot-spot relaxation time. Since the wavelength is determined by the general experimental requirements and the bath temperature tunability is typically a slow and limited process for many cryogenic systems, here we are limiting our study to the bias current dependence of the relaxation time for 1550 nm light at a constant bath temperature of 1.7 K.

Different studies have been performed in the past for determining the hot-spot relaxation time in NbN SNSPDs illuminated under normal incidence, but most of them were limited to a single bias current or a small current range [26,27]. Here we present the results of pump-probe experiments for determining the hot-spot relaxation time in NbN waveguide-integrated SNSPDs over a broad bias current range.

2. Experimental setup

Our device under test (DUT) consists of a 140 nm wide, 40 µm long U-shape nanowire fabricated by patterning a nominal 4 nm thick superconducting NbN film onto a 450 nm thick and 1.5 µm wide single mode waveguide made of stoichiometric Si_3N_4 atop a SiO_2 layer on a bulk Si substrate [7]. We send two photon pulses separated by a variable delay onto the detector. By adjusting the bias current to low values, and by sending a high photon flux to the detector, it is possible to operate the nanowire in the two-photon detection regime [19]. In this way, the first pulse acts as a pump signal, which generates an initial hot-spot region in the nanowire without leading to a breakdown of superconductivity, while the delayed second pulse acts as a probe signal to read out the lifetime of the initial hot-spot. When measuring the detection probability as a function of the delay time between pump and probe pulse, an increased probability of registering a detection event results when the probe pulse reaches the nanowire within the hot-spot relaxation time. The detection probability distribution around the zero-time delay can be approximated by a Lorentzian distribution, whose half width half maximum (HWHM) defines the hot-spot relaxation time [24].

The experimental setup used for our pump-probe experiment is depicted in Fig. 1. The pump and probe pulses are generated by splitting a picosecond laser pulse (PriTel FFL-40M) in two by a 50:50 fiber splitter. The fiber-coupled laser provides optical pulses with 1 ps pulse duration at the DUT, with at a repetition rate of 40.125 MHz. The time delay between the two pulses is set by a calibrated variable fiber optical delay line (General Photonics MDL-002-560ps). The pulses are recombined by a 50:50 fiber splitter and then sent through a set of optical variable attenuators (2 x HP8156A) which are able to reach a maximum attenuation of 120 dB. The attenuated pulses pass through a polarization controller to optimize the transmission through the integrated nanophotonic circuit, which is situated in a helium-4 flow cryostat with a base temperature of 1.7 K.
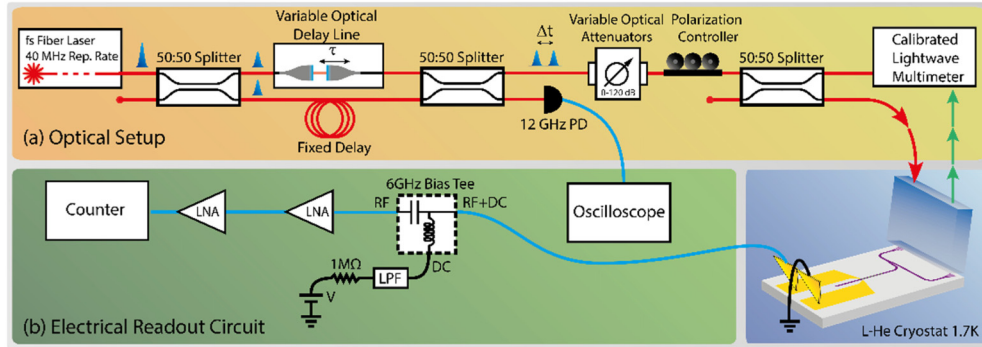
Fig. 1. Schematic of the experimental setup for the hot-spot relaxation time measurement. (a) Optical setup: the two delayed pulses are generated injecting a single laser pulse to a Mach-Zehnder interferometer consisting of two fiber beam splitters and a variable optical delay line. The pump and probe pulses are subsequently attenuated and send to the detector through a nanophotonic calibration circuit at the low temperature stage. A calibrated lightwave multimeter is used to determine the photon flux at the detector. (b) Electrical setup: a stable source is used to bias the detector through a bias tee and two low noise amplifiers are adopted to obtain a detection signal which can be registered by a pulse counter.

The SNSPD is biased through a bias tee (Mini-Circuits ZFBT-GW6 +) by a stable voltage source (Keithley 2400) with a 1 MΩ series resistor. A low-pass filter is inserted in the biasing circuit to further minimize the source noise. The readout circuit consists of two low noise amplifiers (Mini-Circuits ZFL-1000LN +) connected to a frequency counter (Agilent 53230A). In addition, a 12 GHz photoreceiver (New Focus 1554-B) connected to a 6 GHz oscilloscope (Agilent infiniium 54855A) is employed to monitor the zero-time delay position which has been adjusted, using additional fixed fibers segments, at the center of the fiber delay line range. To monitor the number of photons per pulse reaching the detector, a calibrated lightwave multimeter (HP 8135A) is used for measuring the input power and the transmitted optical signal from an on-chip reference port [7]. This allows us to take the variation in coupling efficiency of the focusing grating couplers into account, which depends on the relative position between the fiber array and the grating couplers, and can also vary for different devices due to fabrication imperfections. The average number of photons per pulse m that reaches the detector is calculated by considering the attenuated laser power P_{in}, the femtosecond laser pulse repetition rate RR, the grating coupler coupling efficiency CE, the splitting ratio $S = 0.5$ of the integrated 50:50 Y-splitter, and the waveguide transmission WT, as follows:

$$m = \frac{\lambda}{hc} \frac{P_{in}}{RR} \cdot CE \cdot S \cdot WT \qquad (1)$$

From device characterization and system components stability measurements, the maximum relative uncertainty of the average input photon number m, during the overall measurement time, has been estimated to be 16 %.

3. Detection regime characterization

A preliminary investigation of the detector response is necessary to determine under which working condition SNSPDs operate in the two-photon detection regime. In agreement with our previous experimental results [19], a single-photon source is not needed in order to demonstrate single- and multi-photon capabilities of SNSPDs. It is instead possible to use a strongly attenuated coherent source to measure the detection probability response depending on the input power and thus determine the detection regime of the DUT [11,18,30,31]. The probability of detecting n photons in a coherent state $|\alpha\rangle$ can be described by the Poisson

distribution that, far from the detection probability curve saturation, can be approximated to [32]:

$$DP_n \propto \frac{\left(|\alpha|^2\right)^n}{n!} \qquad (2)$$

where $|\alpha|^2$ is the average number of photons reaching the detector in a limited time-interval which, for pulsed coherent sources, is equal to the pulse duration [19]. By determining the detection probability as the ratio between the measured detector count rate and the pulsed laser repetition rate for known coherent input states, we find that the detection probability depends linearly on the input state (slope 1 in log-log scale) if the detector is sensitive to a single photon ($n = 1$), quadratically (slope 2 in log-log scale) if the detection is sensitive to two photon ($n = 2$), or at higher n-orders (slope n in log-log scale) for n photon threshold detection [26,33].
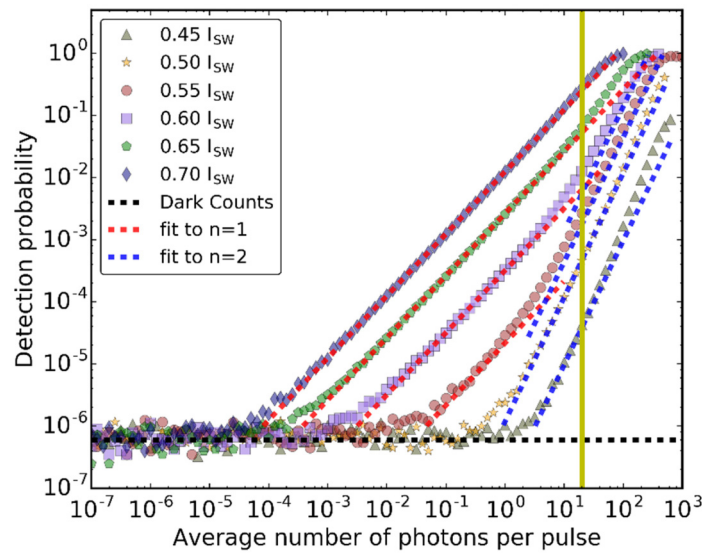

Fig. 2. Detection probability vs average number of photons per pulse at different bias current. The dashed lines represent a fit of the slope of the detection probability curve for single-photon detection regime (red curve) and two-photon regime (blue curve). The horizontal black dashed line indicates the dark count level, which in this current range and is mainly limited by electronic noise and has a constant value of 25Hz. The vertical yellow solid line indicates the average input photon number used for the relaxation time experiment.

The measurement results are depicted in Fig. 2, where it is possible to observe that, from a linear fitting, the detector used in this experiment is capable of two-photon sensitivity in a current range between 0.45 and 0.65 of the switching current I_{SW}.

4. Pump-probe experiment

We performed the pump-probe experiment, keeping a constant illumination of 20 photons per pulse, while changing the bias current from 0.45 I_{SW} to 0.7 I_{SW}. The pump pulse is sent to the detector, while the probe pulse passes through the variable delay line and reaches the detector with a delay of Δt with respect to the first pulse.

The measurement results are shown in Fig. 3. It can be seen that the two-photon detection probability increases for $\Delta t \to 0$. This is expected due to the increased probability for an overlap in time between pump and probe hot-spots when the delay time between the two pulses decreases.
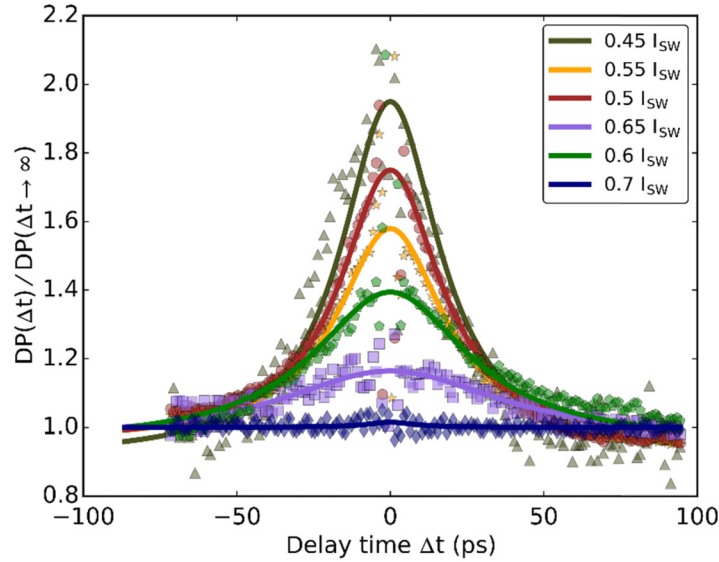
Fig. 3. Normalized detection probability as a function of the pump-probe photon delay time for different bias currents. The fluctuation at $\Delta t \to 0$ is the field autocorrelation trace of the pulsed laser. The solid lines indicate the Lorentzian fit of the measured curves.

5. Discussion

From the pump-probe experiment results, we observe that the increase of the probability is different in both amplitude and time for different bias currents. The amplitude difference can be attributed to the dependence of the detection probability on the photon detection regime of the DUT [24]. If the two pulses reach the detector at the same time (zero delay) far from saturation, the detection probability can be expressed as:

$$DP_n(\Delta t = 0) \propto \eta_n \frac{m^n}{n!} \tag{3}$$

where, differently from [19], η_n denotes a generic efficiency parameter for the n-photon detection regime that was used as a free parameter in our fitting procedure. If the two pulses are separated by a time delay much longer than the hot-spot relaxation time, they can be treated independently and the detection probability is then given by:

$$DP_n(\Delta t \to \infty) = 2 \cdot \eta_n \cdot \frac{\left(m/2\right)^n}{n!} = \frac{1}{2^{n-1}} \cdot DP_n(\Delta t = 0) \tag{4}$$

By dividing the two contributions, we define the detection probability contrast as:

$$\frac{DP_n(\Delta t = 0)}{DP_n(\Delta t \to \infty)} = 2^{n-1} \tag{5}$$

We conclude that the detection probability contrast depends only on the detection regime n within which the detector is sensitive. It is also interesting to note that the detection probability contrast for the same n-photon detection regime is independent of bias current and photon power, unless the variation of those parameters causes a change in the photon number detection regime. Therefore, for $I_b = 0.45\, I_{SW}$, the detector works in a pure two photon regime ($n = 2$), since it shows a count contrast equal to 2. When determining the detection probability contrast at higher bias currents, one can obtain a non-integer number of the detection regime. We attribute this non-integer value to a transition region between

single- and two-photon detection regimes. Inhomogeneity of the wire geometry, leading to the current crowding effect, or the presence of defects in the wire can result to a position dependent sensitivity. At particular bias and illumination conditions it is possible to find sections of the wire that are sensitive to a single-photon and other sections which are sensitive to two-photon, giving a non-integer average detection regime. This behavior is particularly evident in long nanowires and has not been observed in short nanowire detectors, that exhibit a more abrupt detection regime transition [34]. For currents higher than $I_b = 0.45$ I_{SW}, the pump signal has a higher probability of raising a detection event without the assistance of the second pulse absorption. This would mean that the efficiency of the events, which contribute to the pump-probe experiment, becomes lower; nevertheless, the final outcome in terms of relaxation time remains valid and only influences the signal-to-noise ratio.
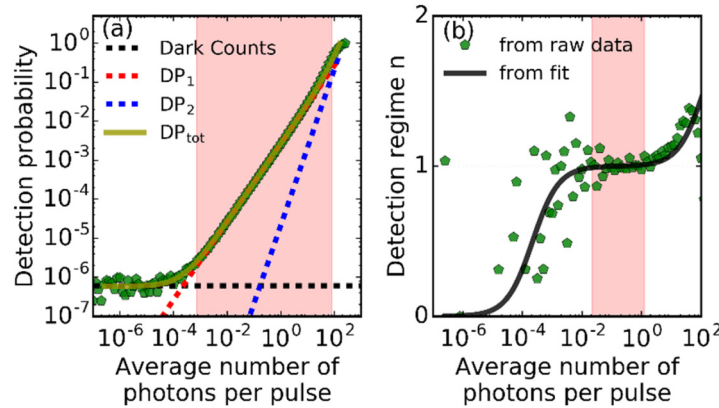

Fig. 4. (a) Detection probability curve fitting result for a bias current of 0.65 I_{SW}, following Eq. (6). The red shaded area represents the pure single photon working regime as defined by the range in which the photon regime dominates aver all the others by 3dB [20]. (b) Reconstruction of the detection regime obtained as the first derivative of the detection probability curve as defined in Eq. (7) for the raw data (dots) and the fitting results (solid line). The red shaded area represents the pure single photon working regime resulting from the calculation of the detection probability derivative. We note that the detector driven at 0.65 I_{SW} can give a single-photon response only in a very small input photon flux range.

In order to exclude artifacts in the different relaxation curve heights and to validate the measurement technique also in a mixed detection regime, we independently reconstructed the expected detection probability contrast by fitting the detection tomography curve (Fig. 2) to extrapolate the photon detection regime n and subsequently using Eq. (5).

The fitting procedure has been performed according to the following equation:

$$DP_{tot} = \sum_n DP_n = \sum_n \eta_n \frac{m^n}{n!}$$ (6)

using η_n as a fitting parameter. The fitting results are reported in Fig. 4(a) where each single DP_n is depicted with dashed lines, while the overall detection probability DP_{tot} is depicted as a solid line. The dark count noise contribution has been included in the fitting, introducing a detection probability DP_0 with $n = 0$.

The detection probability contrast is then calculated using Eq. (5), with n determined as:

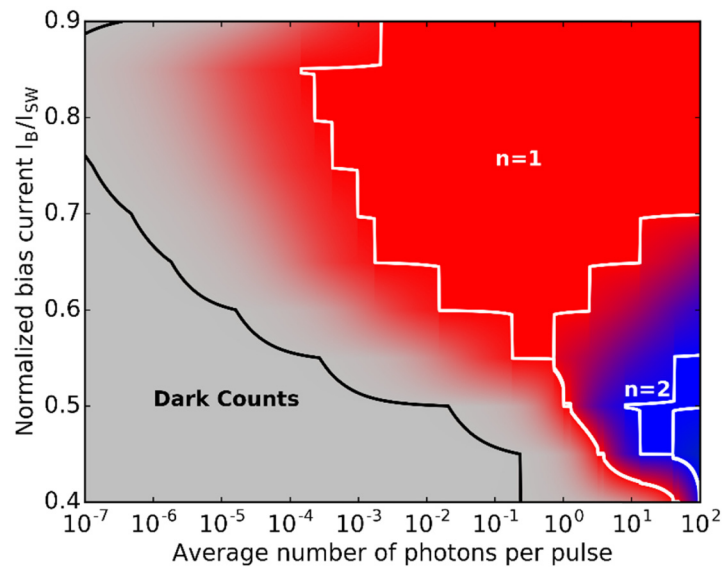$$n = \frac{d(\log_{10}(DP_{tot}))}{d(\log_{10}(m))}$$ (7)

Fig. 5. Tomography of the detection working regimes at different bias currents and illumination obtained applying the fit introduced in Eq. (7). The solid contour lines indicate the pure $n = 0$ (Dark counts), $n = 1$ single-, and $n = 2$ two-photon detection regime. This map allows to have a straightforward understanding of the working conditions which have to be tuned in order to operate the detector in the desired photon sensitivity region. A similar map at different working temperatures and/or at different input photon wavelength could allow to have a complete operative description of the detector.

In Fig. 4(b) we show the extrapolated n from the fitted detection probability and, for comparison, from the measurement data. Both results are in good agreement, and consequently the technique can also be directly applied to raw data, although, the resulting curves would be more affected by noise. This fitting technique can be also adopted as an easy tool to extrapolate the working conditions, in terms of current and illumination, of the detector for the single- or multi-photon regimes. In Figs. 4(a) and 4(b), the red shaded areas represent the illumination range where the DUT acts as a single-photon detector, when operated at $0.65 I_{SW}$. The pure detection regime is typically defined as the working range for which a particular detection mechanism dominates over the others by 3 dB or more [17]. In Fig. 4(a), the red shaded area indicates the pure single-photon regime according to this definition, while in Fig. 4(b) we depict the single-photon regime area obtained by fitting the detection probability contrast. We believe that the latter definition is not only more accurate, since it can be experimentally confirmed by an independent pump-probe measurement, but also can be adopted as an alternative tool for conducting complete tomography of the detector working regimes, as depicted in Fig. 5. Thus, when operating the detector in single- or multi-photon regimes, it is not only fundamental to control the biasing conditions, but also the illumination. We would like to point out that this could represent a limiting factor when the input photon flux is fixed and unknown. Therefore, an operative tomographic calibration of the device would be desirable before proceeding with any other experiment in order to determine a working point which would allow to minimize the contribution of the unwanted regimes.
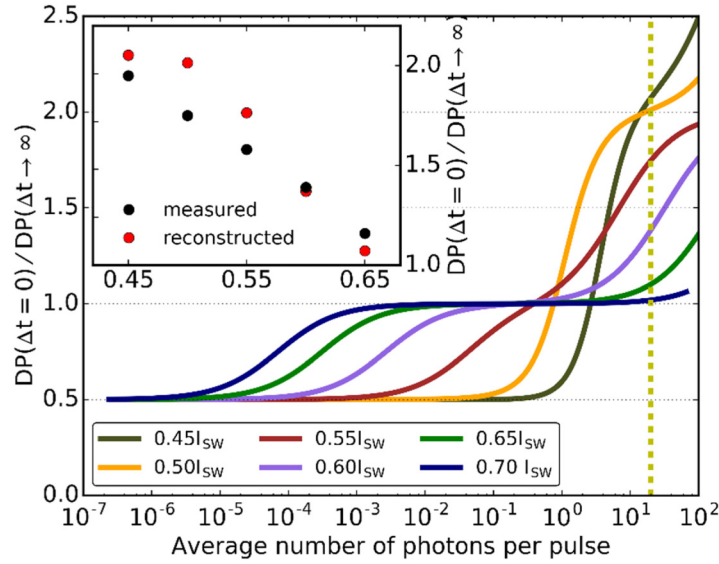
Fig. 6. Reconstruction of the detection probability contrast at different bias currents, obtained by fitting the detection probability curve, as described in Eqs. (6) and (7), to obtain *n* and applying Eq. (5). The inset represents a comparison of measured and reconstructed detection probability contrast, exhibiting a good agreement.

We report in Fig. 6 the reconstructed detection probability contrast at different biasing conditions and illumination. Good agreement between the reconstructed results and the height of the measured relaxation curve in the pump-probe experiment is obtained, as shown in the inset of Fig. 6.

We obtained the hot-spot relaxation time at different bias currents by determining the HWHM of the Lorentzian fit of the detection probability contrast versus delay time curves as shown in Fig. 7. In NbN we observe a strong dependence of the hot-spot relaxation time on the bias current, as reported also for WSi detectors [24], but, according to our quantitative prediction, with a smaller time-scale. The longer time has passed after the absorption of the first photon and the relaxation process, the smaller chance has a second photon to generate a vortex or a VAP and to produce a click. By increasing the bias current further towards the depairing current, even a small concentration of nonequilibrium quasiparticles, which is left over from the first hot-spot, is enough for generating a detection event. From a quantitative comparison between the response of the two materials, it is possible to conclude that the hot-spot recombination in NbN is faster than in WSi [24]. In general, the hot-spot relaxation time is determined by the carrier diffusion $D = L_{th}^2/\tau_{th}$ [35], as well as by the quasiparticles recombination time τ_{rec} [36,37]. Due to the diffusion of the non-equilibrium quasiparticle in the initial phase of the thermalization process, the hot-spot size increases with reduction of the quasiparticle energy down to the superconducting energy gap Δ.

Further hot-spot relaxation is accompanied by a return to the superconducting state, due to quasiparticle recombination:

$$\tau_{rec}^{-1} = \tau_{eph}^{-1} \sqrt{\pi} \left(\frac{2\Delta}{kT_c} \right)^{5/2} \sqrt{\frac{T}{T_c}} \exp\left(-\Delta/kT\right) \tag{8}$$

Considering that the quasiparticle relaxation process occurs in a hot-spot with a temperature $T \approx T_c$, the exponential factor in Eq. (8) has small influence on the recombination rate, thus the electron-phonon interaction time τ_{eph} sets the characteristic relaxation time-scale ($\tau_{rec} \approx \tau_{eph}$). The electron-phonon interaction time in WSi is relatively large ($\tau_{eph} \approx 100$-

200ps) [38] while for NbN this time is on the order of ten picoseconds [39,40]. This allows to predict a slow relaxation process in WSi in comparison with NbN. Furthermore, accounting for the diffusion process gives an increase in the relaxation rate for both materials.
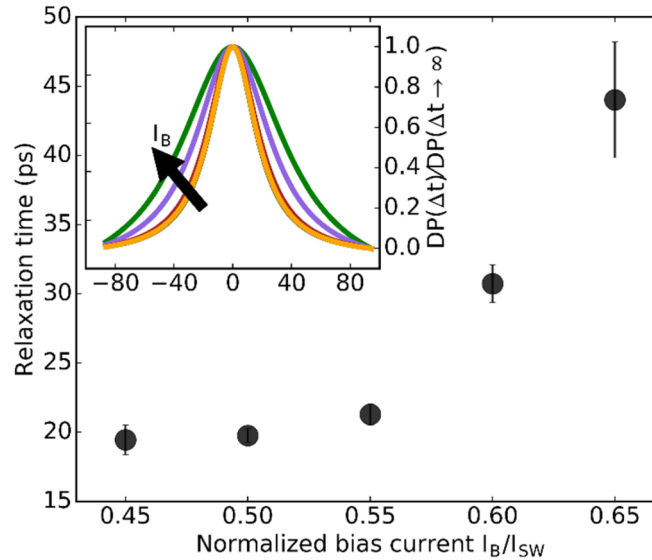

Fig. 7. Hot-spot relaxation time at different bias currents extracted as the HWHM of the Lorentzian fit of the measurement curves presented in Fig. 3. In the inset the fitting results of the 0 to 1 normalized detection probability vs pump-probe delay time are presented. The arrow indicates the increase of the relaxation time with the bias current.

For applications in quantum correlation measurements it is desirable to have short relaxation times, in order to minimize the effect of pile-up with additional photon pairs, especially for sources with fast emission rate or for very small coherence times. On the other hand, WSi detectors have been shown to work in two-photon detection regime over a broader current range and exhibit superior performance in terms of efficiency saturation also in the two-photon regime. It is unknown whether this is related to the detectors' geometry or due to an intrinsic advantage of WSi, considering also its longer hot-spot relaxation time and bigger hot-spot interaction length [24] compared to NbN [25]. In this context, a careful examination of the detector geometry should allow to clarify this aspect.

By determining the relaxation time at $0.5\, I_{SW}$ for several detectors with similar geometry on the same chip, we obtain a relaxation time equal to (22 ± 1) ps, which is in agreement with previous results at the same biasing conditions [26,27].

6. Conclusion

In conclusion, we characterized hot-spot relaxation dynamics in NbN waveguide-integrated superconducting nanowire single photon detectors at different biasing conditions. By adjusting the bias current and the input photon flux, we operated the detector in the two-photon sensitivity regime, where the superconductivity can be broken only if two photons are absorbed within a short timescale, defined by the lifetime of the original excited quasiparticles cloud (hot-spot) in order to have two overlapping excited hot-spots within a spatially limited region of the wire. A pump-probe technique allows us to observe an increase of hot-spot relaxation time with the bias current, which is in agreement with theoretical predictions [29]. Further investigation of the NbN quasiparticle recombination time will allow to design more performant two or more photons single-detector autocorrelators, enabling the implementation of on-chip coincidence measurements of single-photon pairs generated by one or more waveguide-integrated single-photon sources [9] such as CNTs [10]

with only one detector, overcoming the time uncertainty limitations of typical correlation measurement systems.